

Numerical Analysis of Droplet Impact on Liquid Film with Different Surface Structures

Y. Li[†], Y. Lou, Z. He and M. Liu

Faculty of Mechanical and Electrical Engineering, Kunming University of Science and Technology, Kunming, Yunnan Province, 650500, China

[†]Corresponding Author Email: living@kust.edu.cn

ABSTRACT

The collision of droplets with a liquid film is a common occurrence in daily generation. This study uses the CLSVOF approach to analyze a droplet's effect on a liquid film with various trapezoidal surface structures. It analyzes the spray morphology, velocity field, pressure distribution, and the characteristic arguments of the crown and cavity under different trapezoidal widths, heights, and hypotenuse lengths. The findings suggested that growing the height promotes spatter, the collision of droplet with liquid film forms mushroom-shaped velocity region and a zero-velocity region, while generating symmetrical vortices. The area above the trapezoid is identified as a high-pressure region, with its size increasing as the hypotenuse length and trapezoidal width rise and decreasing as the height increases. Three localized high-pressure regions are observed during the impact procedure, and the crown diameter grows with greater height. The bottom diameter of the cavity is influenced by the height, width, and hypotenuse length, with the hypotenuse length exerting the most significant effect. This study provides a theoretical foundation for applying droplet and liquid film collisions.

Article History

Received September 28, 2024

Revised November 25, 2024

Accepted January 3, 2025

Available online March 30, 2025

Keywords:

CLSVOF method

Numerical simulation

Droplet impact on liquid film

Trapezoidal surface

Crown

1. INTRODUCTION

Droplets striking liquid films is a prevalent phenomenon in both natural and manufacturing contexts. This process is not only a classic example of free surface problems but also has significant implications in various fields, including rainfall, agricultural spraying seawater desalination, turbine blade impact, inkjet printing, spraying and coating technologies, and industrial spray cooling (Elhadi & Medraj, 2019; Shi et al., 2022; Zanin et al., 2022; Alessandra et al., 2023; Tsutsumi et al., 2023). When droplets impact liquid films at specific velocities, complex phenomena, such as shape deformation, splashing, diffusion, and penetration, are induced. In practical applications, droplets initially strike solid surfaces, forming thin liquid films. Then, the impact target transitions to this liquid film layer. An in-depth analysis of droplet and liquid film interactions directly influences the optimization of spray and coating technologies, which are extensively utilized in the manufacturing, automotive, and aerospace industries. Understanding these mechanisms can enhance spraying processes, improve coating uniformity and adhesion, reduce material wastage, and elevate product quality. The deformation and cavity morphology of liquid films resulting from droplet impacts

provide essential insights for designing more impact-resistant and corrosion-resistant membrane materials, extending the lifespan and reliability of seawater desalination equipment. In addition, data on velocity fields and pressure distributions during droplet impacts on liquid films are critical for designing more efficient and stable nozzle shapes. Such improvements enhance cooling efficiency, reduce energy consumption, improve print quality, and minimize spatter. A fuel injection system is critical in internal combustion engines and gas turbines (Lin et al., 2023). The interaction between droplets and liquid film directly affects fuel atomization and mixing, influencing combustion efficiency and pollutant emissions. Hence, studying droplet impact processes is essential for developing more efficient fuel injection systems, improving combustion performance, and reducing environmental pollution. The liquid film formed by droplets striking heated surfaces in spray cooling systems significantly enhances heat transfer efficiency. This improvement is crucial for advancing cooling technologies to meet the heat dissipation demands of high-power-density electronic devices. Similarly, droplet and biofilm interactions are pivotal in drug delivery and medical nebulizer design (Ochowiak et al., 2017; Panzade et al., 2024). Optimizing nebulizer design and operating

NOMENCLATURE			
α	volume fraction	ρ	density
Φ	level set function	σ	surface tension
τ	non-dimensional time	H_r	Crown's height
δ	distance function	g	gravitational constant
v	velocity at the moment droplet contacts liquid film	V_2	total volume of unit
p	pressure	\vec{n}	interface normal vector
c	length of the hypotenuse of the trapezoid	H^*	non-dimensional depth of the liquid layer
T	temperature	R_e	Reynolds number
H	depth of the liquid layer	\vec{F}_s	force caused
c^*	length of the dimensionless hypotenuse	W_e	Weber number
a	width of the trapezoid	a^*	non-dimensional width
b	height of the trapezoid	h	Crown's height
V_1	volume of certain fluid	k	curvature
D_d	droplet diameter	D_r	Crown's diameter
d	bottom diameter of the cavity	t	time
b^*	non-dimensional height	R	Crown's radius

parameters can improve drug distribution and absorption within the body, ultimately enhancing treatment efficiency and patient experience. Accordingly, studying droplet impact on liquid films is vital for optimizing equipment design, material selection, and process parameters across technologies such as spraying equipment, desalination equipment, jet cooling systems, inkjet printing devices, and turbine blade cooling systems. These advancements enhance equipment efficiency and performance, lower costs, reduce environmental pollution, and offer substantial practical and application value.

The study of droplet collision with a liquid can be classified into three categories: conceptual analysis, laboratory investigation, and computational modeling. Currently, the prevalent methods for studying fluids include the lattice Boltzmann method (LBM), the volume of fluid method (VOF), and level set method (LS) (Hirt, 1981; Osher, 1988; Fallah et al., 2016). Sussman proposed a simulation method that couples VOF and LS, known as the coupled level set and volume of fluid method (CLSVOF) (Sussman, 2000). This strategy is broadly recognized in modeling the phenomenon of droplet striking liquid surfaces. For instance, some researchers utilized the CLSVOF to mimic the crash of a droplet and liquid surface, and another researchers utilized CLSVOF to explore the evolution process of double droplet and liquid film (Guo et al., 2015; Liang et al., 2021). The collision interaction of two droplets on curved surface was investigated through experiments, and elaborated the effect of curvature radius on droplet interaction (Chen et al., 2024). The VOF was used to study internal flow mechanisms of turbines (Lu et al., 2024). The phenomenon of twin droplet oblique collision with a liquid film was examined and discovered that cylindrical jets produced by symmetrical inward impacts are more prone to break (Tao et al., 2022). The experimental findings indicated that when the impact angle exceeds 30°, the splatter phenomenon is suppressed, and as the angle of impact rises, the elevation of the crown progressively diminishes. Manzello and Yang (2002)

analyzed droplet impact dynamics, asserting that different impact targets yield varying droplet dynamics. Therefore, the dynamic characteristics of the droplet alter with changes in the impact target. In real-world applications, however, surfaces impacted by droplets are not always smooth and ideal; irregular surfaces are common, and droplet impacts on different surfaces have distinct effects on the evolution law. Hu et al. (2022, 2024) and Peng et al. (2023) studied the phenomenon of droplet impact on superhydrophobic surfaces. The effects of droplet collisions with a hot surface was studied, noting the depression of the central thin section of the capillary (Palmetshofer et al., 2024). Subedi explored the interaction between hot surfaces and droplets, and Agrawal et al analyzed the phenomenon of droplets colliding with surfaces at different contact angles (Kshitiz & Song-Charng, 2022; Agrawal et al., 2023). Liu et al. (2024) found that the diffusion time of droplets varies with surface temperature, and colder surfaces often reduce the behavior of droplets. Li et al. (2010) conducted research on the influence of water droplets striking textured surfaces, with their experimental results showing that the solid fraction influences the contact time. Hong and Wang (2017) analyzed the effects of curvature on a spherical liquid film by studying the procedure of a pair of droplets hitting it. They found that the average wall heat transfer coefficient increased with the sphere's curvature. In contrast, the average wall heat density of a flat liquid film was lower than that of a spherical one. A study analyzed the projectile impact process through numerical simulations and concluded that temperature is critical in the high-speed water intake process (Yang et al., 2024). Researcher found that the bounce dynamics of droplets impacting cylindrical leaves are asymmetrical, and this bounce asymmetry reduces contact time (Liu et al., 2015). Yonemoto et al. (2022) predicted whether droplets would splash upon hitting a solid matrix, and Yada et al. (2022) studied have a effects on droplets surfaces and tilted microcolumns. Rajendran et al. (2023) predicted splashing and non-splashing outcomes using five different liquids on the impact of droplets on liquid films. Bird et al. (2013) conducted experiments on droplet impacts on

the asymmetric surfaces of spine structures, finding that such impacts on asymmetric surfaces reduced the total contact time. However, they did not consider the collisions and interactions between droplets and liquid films with surface microstructures, which indicates that the progression of droplet collisions on liquid layer with varying wall warrants additional investigation.

Currently, various simulation methods are employed to explore the effects that the collision of droplets with the liquid stratum, focusing primarily on factors such as depth of liquid layer, droplet diameter, and velocity of contact point. Few studies have explored droplet impacts on liquid films with varying surface structures. This study aims to address this gap, particularly under non-ideal surface conditions. An in-depth analysis of this phenomenon could enhance the optimization of technological processes, for instance, coating technologies and digital inkjet technology, improving product quality and production efficiency. In addition, it can deepen our understanding of complex behaviors like fluid deformation, splashing, and diffusion within fluid mechanics. The study's findings are of theoretical significance and have extensive potential applications in advancing industrial technology, conserving resources, and protecting the environment. They provide theoretical support for the application of droplet collision with liquid films. This study establishes a model of water-drop striking liquid membranes with diverse trapezoidal surface structures. The CLSVOF approach is employed for the analysis of effects of the width, height, and hypotenuse length of trapezoidal surface structures on droplet impact on liquid films. It is possible to control the diffusion and absorption behavior of droplets on liquid films, which is crucial for designing novel liquid handling and distribution systems by studying the development of crowns. The correctness of the research model was additionally validated.

2. MODELS AND SIMULATION METHODS

2.1 Establishment of Models

In our study, the influence of gravity was considered. We analyzed the procedure that a one droplet hitting liquid layer with different trapezoidal surface structures, and the 2D physical model is shown in Fig. 1. In the figure, D_d is the droplet diameter, v represents the instantaneous

velocity speed that the droplet contacts liquid film, the surface structure is a trapezoid, a is the trapezoid's width, a^* is non-dimensional width, $a^* = a/D_d$. b is the trapezoid's height, non-dimensional height, $b^* = b/D_d$. c is the hypotenuse of the trapezoid, c^* represents the length of the non-dimensional hypotenuse, and $c^* = c/D_d$, H represents the extent of the fluid layer's vertical measurement, H^* signifies the non-dimensional depth of the liquid layer.

2.2 The Approach of Numerical Simulation

This research modeled the collision that droplet with liquid film atop trapezoidal surface, which is complex and includes changes in the gas-liquid two-phase interface. Therefore, it is the most critical simulation process that captures the boundary between gas and liquid phases. CLSVOF method combines the advantages, using the Level Set function to improve the interface resolution and the volume fraction field of VOF to ensure volume conservation (Olsson & Kreiss, 2005; Olsson et al., 2007). This approach successfully captures the boundary between gas and liquid phases.

Volume fraction is commonly used to accurately track and describe the spatial distribution of different fluids within a computational domain. It refers to the proportion of the volume of a certain fluid (V_1) to the total volume of unit (V_2) in the computational domain, and α is defined as follows:

$$\alpha = \frac{V_1}{V_2} \tag{1}$$

$\alpha = 1$ represents a unit entirely filled with liquid, while $\alpha = 0$ indicates a unit filled with gas, and $0 < \alpha < 1$ represents gas-liquid interface. The master equation for the volume fraction is given by:

$$\frac{\partial \alpha}{\partial t} + v \cdot \nabla \alpha = 0 \tag{2}$$

Φ is level set function, $\Phi = 0$ is applied to denote the interface, with the governing equation formulated as:

$$\frac{\partial \Phi}{\partial t} + v \cdot \nabla \Phi = 0 \tag{3}$$

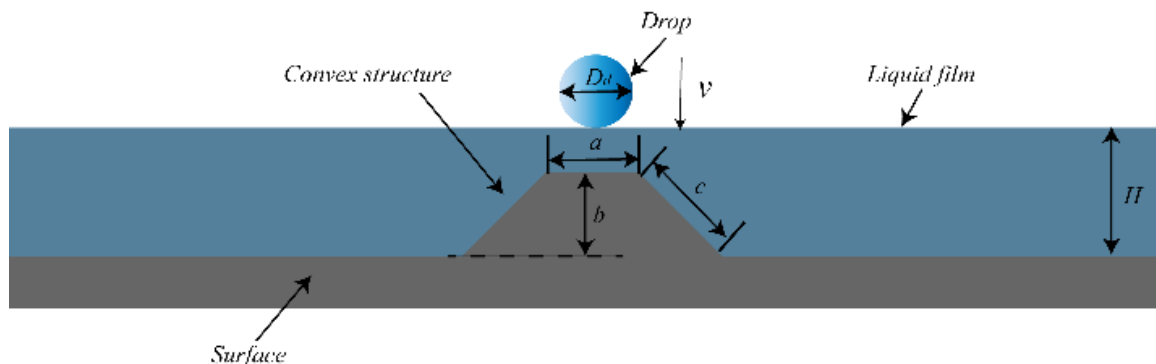


Fig. 1 Schematic diagram of two-dimensional model

Treating water and air as incompressible Newtonian fluids, fluid dynamics are solved by solving the Navier-Stokes (N-S) equation, which is given by equations (4), and the continuity equation is (5).

$$\rho \frac{\partial v}{\partial t} + \rho \nabla \cdot (v v) + \nabla p = \nabla \cdot \mu \left[\nabla v + (\nabla v)^T \right] - \vec{F}_s + \rho g \quad (4)$$

$$\nabla v = 0 \quad (5)$$

where P denotes pressure, T signifies temperature, ρ represents density, t refers to time, and g is the constant about gravitational acceleration.

$$\vec{F}_s = \sigma k \delta \nabla \Phi \quad (6)$$

where \vec{F}_s is the force resulting from surface tension, δ is distance function, and σ is surface tension. The curvature k is defined as follows:

$$k = \nabla \cdot \frac{\nabla \Phi}{|\nabla \Phi|} \quad (7)$$

The interface normal vector is shown in equation (8).

$$\vec{n} = \frac{\nabla \Phi}{|\nabla \Phi|} \quad (8)$$

This study utilizes finite element analysis software ANSYS2021 to resolve the pressure-velocity coupled equations with the PISO algorithm. The gradient is computed through a cell-based least squares approach, pressure estimation employs the body force-weighted technique, momentum computation applies the second-order upwind method, and volume fraction is derived through geo-reconstruct procedure, and the simulation employs a time step of 0.00001 seconds, totaling 2500 steps. Rectangular region measuring 40×30 mm is computational domain, in which the gaseous phase is consisted by air, while the liquid phase is composed via water. The air density is 1.225 kg/m³ and viscosity

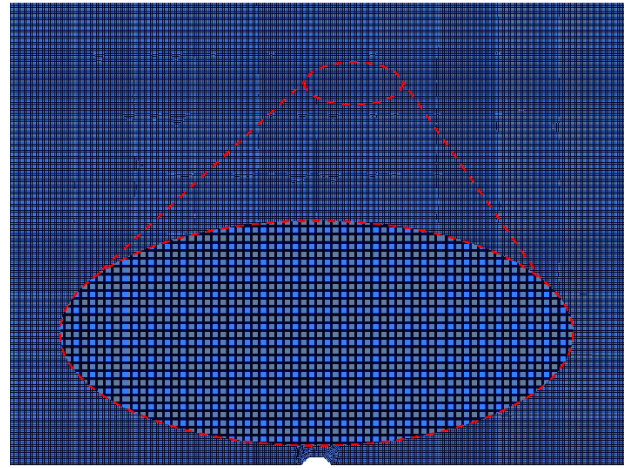


Fig. 2 Grid diagram. (The dashed area is a local enlarged grid)

coefficient is 1.789×10^{-5} Pa·s. while water viscosity is 0.001 pa·s, accompanied by density of 998.2 kg/m³. The Weber number (W_e) at 246, the contact angle measures 90°, the Reynolds number (R_e) at 5971. Surface tension is 0.072 N/m. The lower boundary of the computational domain is established as a non-skid boundary, and the other edges are designated as pressure outlets. Mesh adaptive technology is employed to refine the local mesh and enhance simulation accuracy (Theodorakakos & Bergeles, 2004). The grid count during the calculation process reaches 120,000. The grid diagram is depicted in Fig. 2.

Grid independence verification is performed to confirm that the simulation outcomes are unaffected by the discretization scale. The results are displayed in Fig. 3(a). Characteristic parameters over time at 2.5, 3.5, and 4.5 ms are selected for verification, using the crown diameter (D_r) as the characteristic parameter. Typically, the deviation between two consecutive calculations ranges between 5% and 10%. It can be concluded that the mesh size has no effect on the simulation results. Figure 3(a)

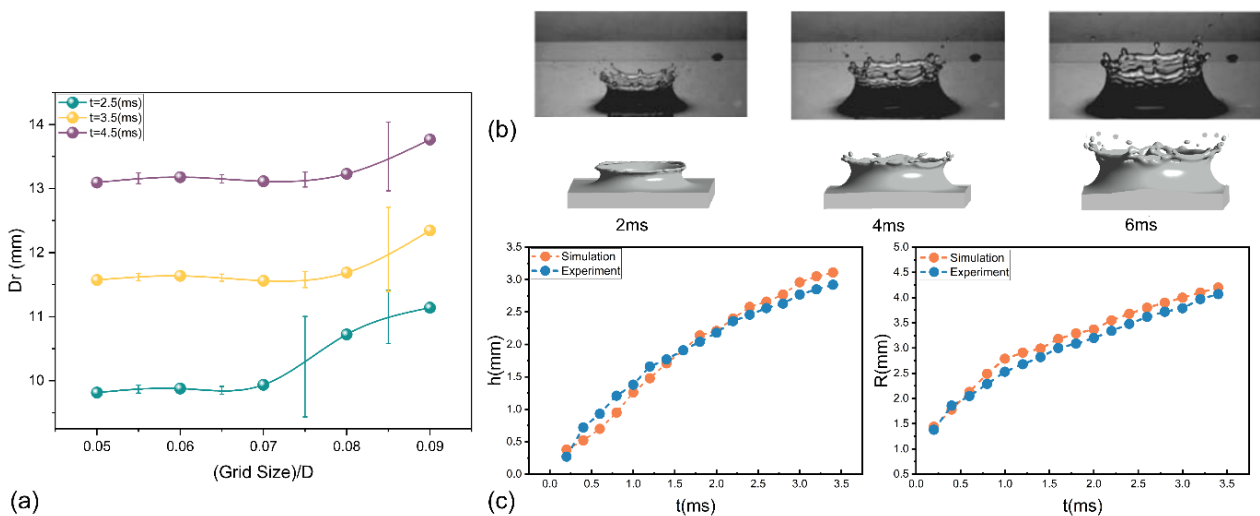


Fig. 3 Checking the model's accuracy levels: (a) Confirmatory analysis for lattice independence; (b) Study of the spray pattern's morphological features; (c) Quantitative validation assessment

Table 1 Arguments employed in the simulation

D_d (mm)	H^*	a^*	v (m/s)	b^*	c^*
2	1	0.25–0.75	3	0.25–0.75	0.75–1.75

indicates that when the mesh size to droplet diameter ratio exceeds 0.07, the characteristic parameters exhibit significant variability, and the deviations are outside the acceptable error range. When the ratio is 0.07 or lower, the characteristic parameters remain stable despite changes in mesh size (within the acceptable error range). Therefore, the initial mesh size is set at 0.05 times the droplet diameter to optimize the accuracy of the simulation in this study.

A set of experimental data from Okawa et al. was selected ($v = 3.3$ m/s, $D = 4.5$ mm, $H^* = 0.45$) to verify accuracy of spray results simulated by the mode (Okawa et al., 2006). The outcomes are depicted in Fig. 3(b). The spray patterns produced by the simulation align closely with the experimental results. Another set of experimental data was selected from Chen et al. (2020) for quantitative verification ($v = 3.08$ m/s, $H = 1.45$ mm, $D = 2.33$ mm). And these results are illustrated in Fig. 3(c), where h represents the crown's height ($h = H_r$) and R denotes the radius of crown ($R = D_r/2$). The outcomes of the simulation align well with the empirical data. Therefore, the physical model adopted in this study and the CLSVOF approach is capable of precisely mimicking the procedure of a droplet striking a liquid layer.

3. RESULTS AND DISCUSSION

This study uses the CLSVOF approach to model the collision of an individual droplet against a liquid film with different trapezoidal surface structures. The non-dimensional parameters that must be considered in the numerical simulation are Re , We , non-dimensional liquid layer depth H^* , non-dimensional time τ and three characteristic parameters (a^* , b^* and c^*) of dimensionless trapezoid. These parameters are defined as follows:

$$Re = \frac{\rho D_d v}{\mu}, We = \frac{\rho D_d v^2}{\sigma}, H^* = \frac{H}{D_d}, a^* = \frac{a}{D_d}, \tau = \frac{tv}{D_d}, b^* = \frac{b}{D_d}, c^* = \frac{c}{D_d} \quad (9)$$

The relevant parameters used in the simulation process are listed in Table 1.

Figure 4 depicts the definition of the key attributes for the crown and cavity. D_r is the crown's diameter, the diameter at the base of the cavity, denoted as d , represents the horizontal measurement across the cavity's lowest point, H_r indicates the elevation of water splashes: the vertical separation between the peak of water splashes and the horizontal plane of the wall.

3.1 The Influence of Width During Collision Process

Figure 5 illustrates the visualization results of the effects of different widths about droplet impact on a liquid layer, where values of a^* are 0.25, 0.5, and 0.75, respectively. In Fig. 5(a), the velocity vector cloud map at

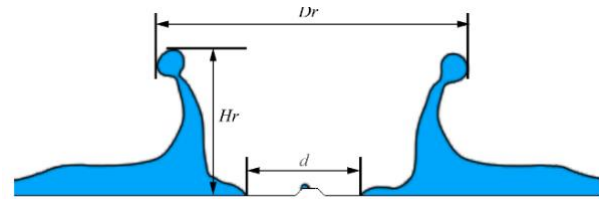


Fig. 4 Schematic diagram of crown and cavity

time $\tau = 0.75$ is displayed, with gray lines representing the interface. Upon the initial impact of the droplet on the liquid layer, the transformation of impact kinetic energy into liquid potential energy forms a mushroom-shaped velocity region near the trapezoidal structure. Due to the symmetry of the trapezoidal structure, the pressure gradient and velocity field of the fluid are arranged on either side of the structure symmetrically, with the maximum velocity region arranged on either side of the crown symmetrically. During impact, momentum flows symmetrically on both sides of the impact point, while surface tension drives the liquid outward from the impact point. Trapezoidal geometry affects the return path, causing the air around the droplet to be squeezed, forming a high-pressure zone. Hence, the high-pressure air flows toward the low-pressure zone, forming two symmetrical and opposite eddies on both sides of the droplet. The vortex center is located at the top of the crown and directly above the trapezoid. The vortex forms a symmetrical rotational flow positioned to either side of the impact point. However, due to the mutual cancellation of the flow direction, a region of zero velocity is established at the core of the impact point. As the width increases, the hit force engendered by the droplets on the liquid layer diminishes, and the kinetic energy possessed by the droplets gradually reduces, leading to an expanding area of the liquid film with zero velocity. Therefore, the expansion of the width corresponds to an enlargement of the zero-velocity area. The impact velocity below the liquid layer forms radial velocity and oblique upward velocity on the trapezoidal structure. In contrast, at the edge, partial velocity interacts with the boundary between gas and liquid, and the velocity direction changes, resulting in the oblique downward velocity. Figure 5(b) depicts the influence of width on spray morphology. Spray morphology remains essentially similar despite changes in width, which has little effect on spray morphology. However, at $\tau = 0.75$ the bottom of the cavity becomes flatter as the width increases. Figure 5(c) shows the pressure distribution under different width conditions. At the initial moment of impact, there is a high-pressure region directly above the trapezoid, and the area and pressure value of the high-pressure region increase as the width grows, with the pressure at interface approaching atmospheric pressure. With continuous collision process, when $\tau = 1.5$, the liquid on the trapezoid surface converts to the bottom of the trapezoid

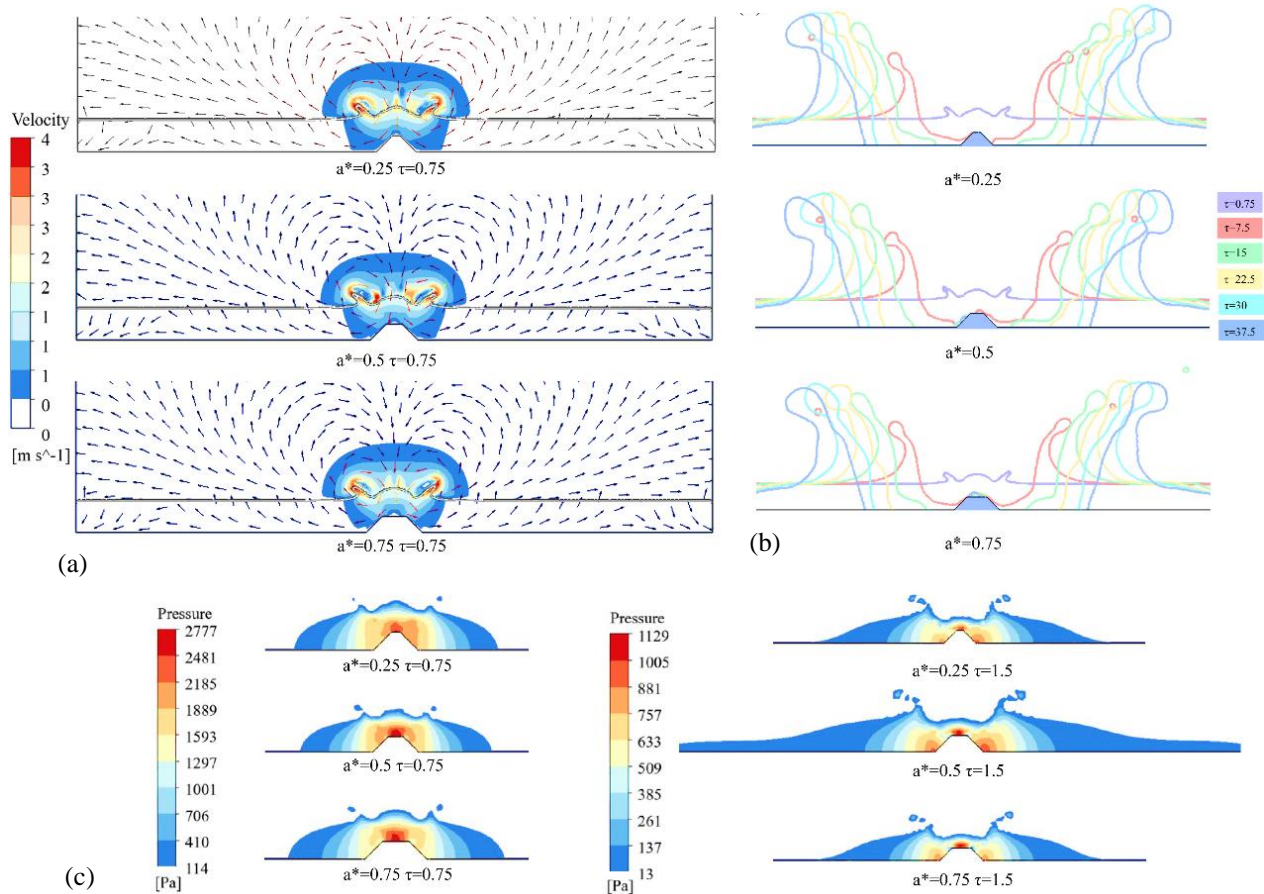


Fig. 5 Influence of width during collision process: (a) Velocity vector cloud diagram; (b) Schematic diagram of spray form; (c) Pressure distribution diagram

under the action of surface tension, and the high-pressure zone transforms into three local high-pressure zones, which are located at the two angles above the trapezoid and at the bottom.

3.2 The Effect of Height During Collision Process

Figure 6 presents this research result which the influence about diverse heights on droplet hit a liquid film, where the values of b^* are 0.25, 0.5, and 0.75, respectively. The velocity vector cloud image at Fig. 6(a) illustrates the droplet impacting the liquid film at $\tau = 0.75$, with gray lines representing the interface. Figure 6(a) reveals that it is same as patterns between the changes of velocity vector and the influence of width on the velocity vector exhibit similar under different height conditions. However, as the height increases, the force exerted by the droplet on the liquid film increases, with the droplet carrying a greater amount of kinetic energy. Therefore, in the zero-velocity region, the liquid film gains velocity, so exits the zero-velocity region, reducing the area of the zero-velocity region directly above the trapezoid. Figure 6(b) demonstrates that height significantly affects spray morphology. Upon collision with the liquid film, a fraction of the droplet's kinetic energy is conveyed to the liquid film, causing deformation and splashing. As the height increases, the degree of splashing intensifies, and the count of additional droplets formed also increases (Wang & Chen, 2000; Wal et al., 2005). This is because a

greater height results in a stronger impact force and more kinetic energy carried by the droplet, leading to more severe deformation of the liquid film and a more intense splashing effect. In contrast, the surface tension on the droplet is relatively reduced, resulting in a sharper cavity bottom. The shape gradually evolves into a 'W' shape. Finally, Fig. 6(c) demonstrates that at $\tau = 0.75$, as the height increases, the area of the high-pressure region formed directly above the trapezoid gradually decreases. When $b^* = 0.75$, the shape of the high-pressure region transitions from a square to an oval, and eventually, only one local high-pressure point remains. When $\tau = 1.5$ and $b^* = 0.75$, the high-pressure region directly disappears above the trapezoid.

3.3 The Effect of Hypotenuse Length During Collision Process

Figure 7 illustrates the influence that diverse hypotenuse lengths on droplet collision with a liquid film, with c^* values set at 0.75, 1.25, and 1.75. In Fig. 7(a), the velocity vector cloud image at $\tau = 0.75$ provides a visual representation of the waterdrop's interaction with the liquid surface. Although the change in velocity vector under different hypotenuse lengths resembles the effect of varying widths and heights, the area of the zero-velocity region also expands with increasing hypotenuse length, albeit not as significantly as changes in width. Figure 7(b) indicates that at $\tau = 7.5$, an increase in hypotenuse length

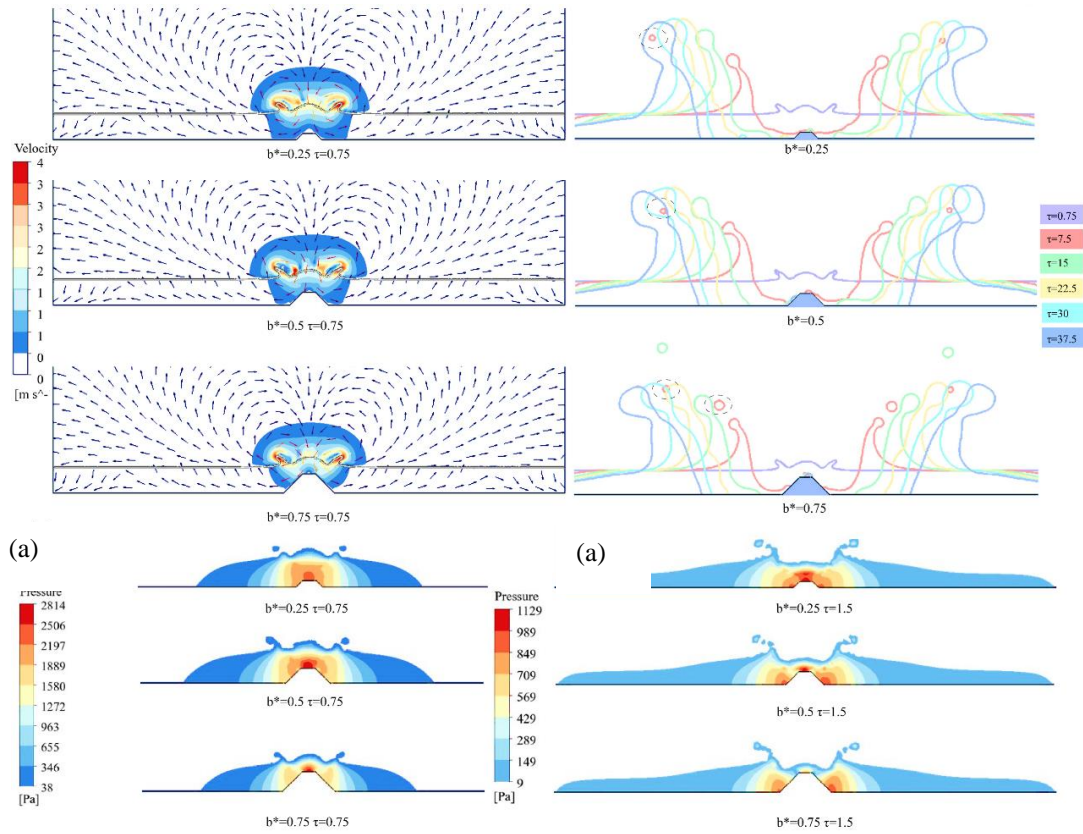


Fig. 6 Influence of height on the impact process: (a) Velocity vector cloud diagram; (b) Schematic diagram of spray form; (c) Pressure distribution diagram

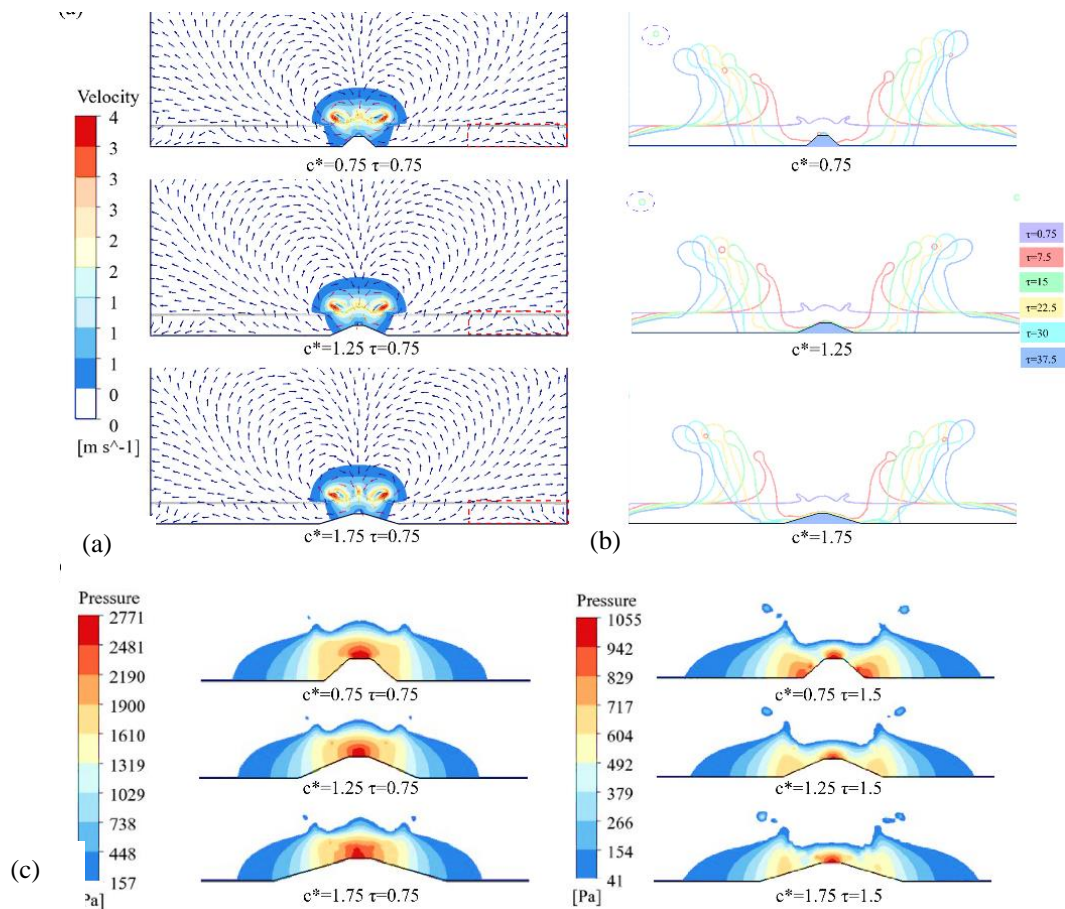


Fig. 7 Influence of hypotenuse length during collision process: (a) Velocity vector cloud diagram; (b) Schematic diagram of spray form; (c) Pressure distribution diagram

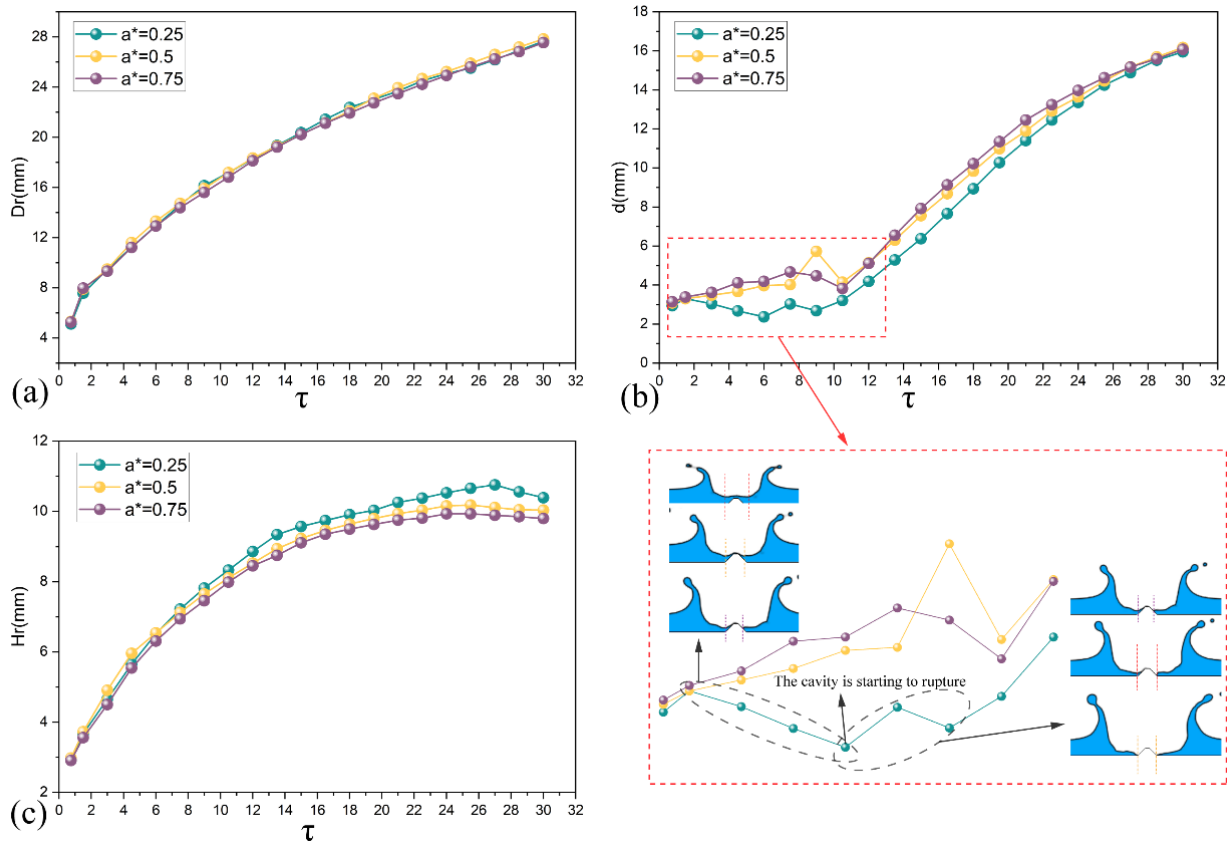


Fig. 8 Influence of different widths on characteristic parameters: (a) Crown diameter; (b) Base diameter of the cavity; (c) Crown height

leads to more droplet kinetic energy being converted into potential energy, decreasing droplet velocity. This reduction in velocity diminishes the shear and impact forces between the droplet and the inclined plane, reducing the force of impact on liquid film and cavity's base. Simultaneously, with the contact area increases between the droplet and inclined plane, and surface tension on the droplet increases, reducing the degree of droplet deformation and facilitating the maintenance of its original shape. These factors flatten the cavity's bottom and create a "u" shape. The influence of hypotenuse length on the bottom of the cavity is more significant than that of width. Figure 7(c) shows that at $\tau = 0.75$, a high-pressure area forms directly above the trapezoid. As the hypotenuse length increases, the area of this high-pressure region expands, but the radial extension of the low-pressure region contracts. At $\tau = 1.5$, the pressure decreases rapidly, especially at $c^* = 1.25$ and $c^* = 1.75$, where only the local high-pressure area directly above the trapezoid remains, with high-pressure areas at the bottom two corners disappearing.

3.4 The Effect of Width on Feature Parameters

Figure 8 illustrates the change in the crown and cavity characteristic parameters that have non-dimensional time under various width conditions (a^* is 0.25, 0.5, 0.75, respectively). Figures. 8(a) and 8(c) reveal the influence of various widths on the diameter and height in the crown. It can be interpreted that the diameter of the crown is almost unaffected by the change in width, and the

diameter of the crown is roughly the same under different width conditions from Fig. 8(a), a conclusion also obtained by Lin et al. (2022). Figure 8(c) depicts that when $a^* = 0.75$, the crown's height remains minimal. At the commencement of the collision, the width has little effect on the height of water splashes. However, with continuous impact, after $\tau = 7.5$, the crown's height begins to decline as the width increases. The height of the crown begins to decline after it peaks and then decreases most rapidly when $a^* = 0.25$. Figure 8(b) shows that the width significantly influences the cavity's bottom diameter. In the cavity rupture stage, the bottom diameter of the cavity decreases due to the change of the bottommost point of the cavity. When $a^* = 0.25$, the deepest point at the base of the cavity first touches the trapezoidal structure, marking the moment the cavity begins to break. The following descent is due to the liquid residue on the trapezoid surface. As the impact continues, this residual liquid pools under surface tension to the very bottom, triggering a second drop in the diameter of the cavity (at which point the entire trapezoidal structure is exposed to air). At the end of the cavity rupture stage, the cavity's base diameter expands in tandem with the width, but the influence of the width change on base diameter of the cavity is gradually weakened with time (for $a^* = 0.5$ and $a^* = 0.75$, the lowest drop in cavity bottom diameter occurs at the end of the cavity rupture).

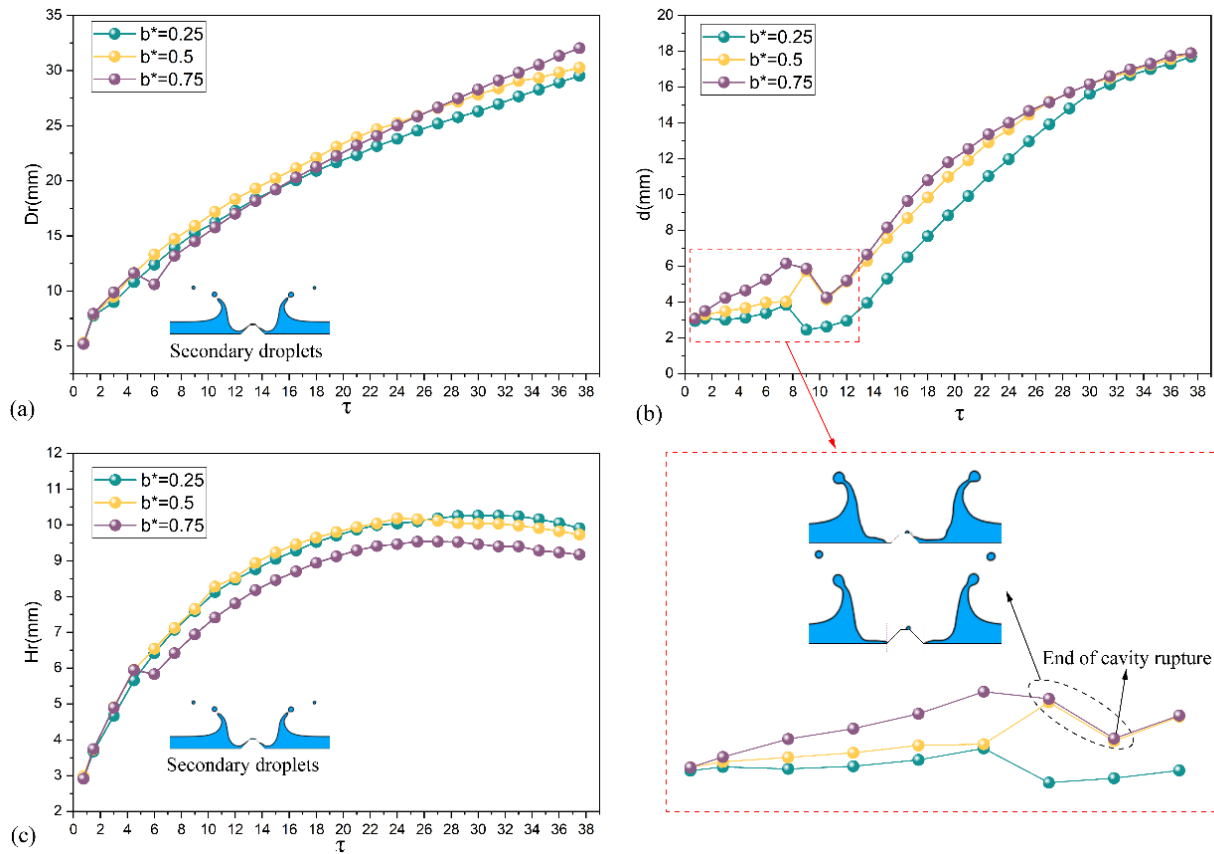


Fig. 9 Influence of different heights on characteristic parameters: (a) Crown diameter; (b) Base diameter of the cavity; (c) Crown height

3.5 The Effect of Height on Feature Parameters

Figure 9 illustrates the changes of water splashes and cavity features parameters with non-dimensional time under different height conditions (b^* is 0.25, 0.5, 0.75, respectively). Figures. 9(a) and (c) demonstrate the influence of varying heights on the diameter and height of the crown. Figure 9(a) indicates that the diffusion of the crown primarily depends on the striking force of the droplet against the liquid membranes. This force intensifies with the rise in height, significantly influencing the crown's diameter. As the height increases, the impact force on the liquid membranes intensifies, the spattering is more severe, the crown's diameter decreases are caused by the formation of secondary droplets. However, at $b^* = 0.75$, the crown diameter increases most rapidly. During the latter stages of the impact phenomenon, the diameter of crown also shows an upward trend as the height increases. Figure 9(c) indicates that height greatly influences the height of water splashes. Before the generation of secondary droplets, height exerts a minimal impact on crown's height. However, after secondary droplets form, the crown's height decreases with an increase in height before reaching its maximum, [Guo et al. \(2021\)](#) also came to the same conclusion. When $b^* = 0.75$, the crown's height is at its lowest. Figure 9(b) reveals that height also significantly affects the bottom diameter of the cavity, with a variation pattern similar to that of the width's influence on the bottom diameter. After cavity rupture, the bottom diameter increases with height, but the

effect of height on the bottom diameter gradually diminishes over time. However, at $b^* = 0.25$, unlike the width's influence, the bottom diameter of the cavity does not show a double decrease, and its lowest point is consistent with that observed during the width change (at $b^* = 0.25$, the lowest point occurs when the cavity begins to rupture; at $b^* = 0.5$ and $b^* = 0.75$, it occurs at the end of the cavity rupture).

3.6 The Effect of Hypotenuse Length on Feature Parameters

Figure 10 shows the variation of crown and cavity characteristic parameters with non-dimensional time under different hypotenuse lengths (c^* is 0.75, 1.25, 1.75, respectively). Figures. 10(a) and 10(c) illustrate the influence of different lengths on diameter and height of water splashes. Figure 10(a) indicates that the hypotenuse length exerts minimal influence on the crown diameter. Figure 10(c) demonstrates that before the crown height runs to its peak, it is at the lowest level when $c^* = 1.25$, and as hypotenuse length rises, height of water splashes first decreases and then increases. Before cavity ruptures, the base diameter of the cavity increases with the hypotenuse length. However, as the hypotenuse length increases, the cavity's bottom diameter decreases after the cavity fractures. At $c^* = 0.75$, the lowest point of decline occurs when the cavity begins to rupture, and at $c^* = 1.5$ and $c^* = 1.75$, it occurs at the end of the cavity rupture.

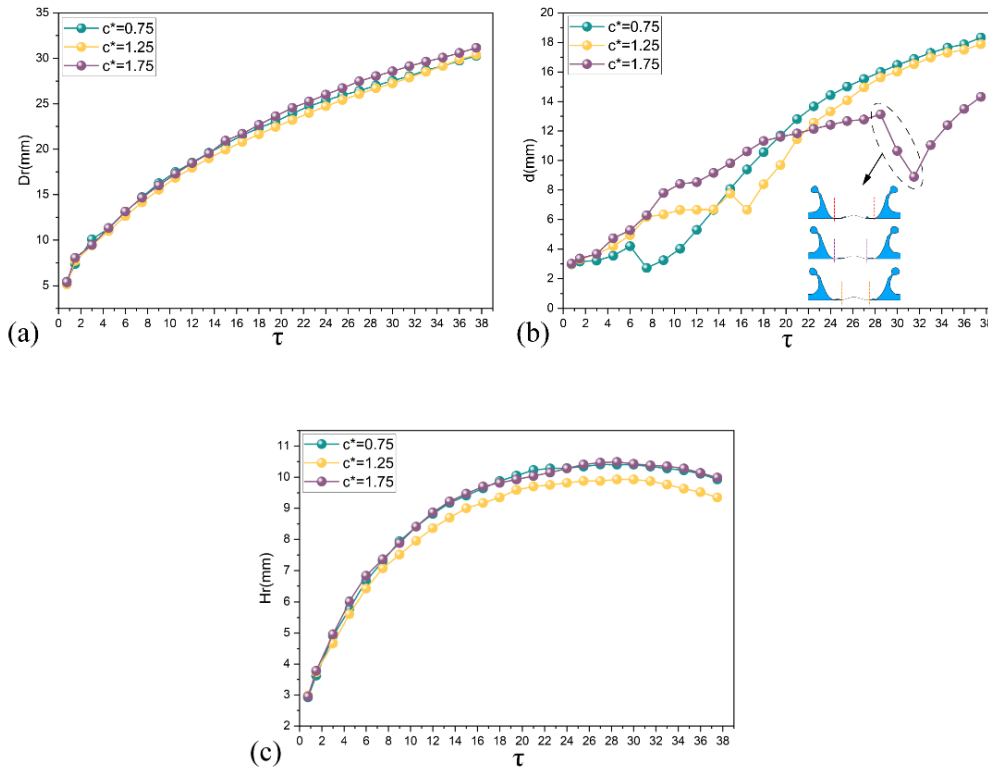


Fig. 10 Influence of different hypotenuse lengths on characteristic parameters: (a) Crown diameter; (b) Base diameter of the cavity; (c) Crown height

4. CONCLUSION

This study establishes a numerical model of a single droplet impacting a liquid film with different trapezoidal surface structures. The processes of droplet impingement and crown development are analyzed. The following conclusions are drawn:

1. The effects of width, height, and hypotenuse length on velocity exhibit common and distinct characteristics. These factors all lead to a mushroom-shaped velocity region. Directly above the trapezoid, a zero-velocity region appears; two eddies in opposite directions are formed symmetrically. Below the liquid film, there is an oblique downward velocity. The area of the zero-velocity region increases with the width and hypotenuse length, with the influence of width on this region exceeding that of the hypotenuse length. In contrast, the area decreases with an increase in height.

2. Effects of width, height, and hypotenuse length on spray morphology: The change in height significantly influences the spray morphology, and increasing the height exacerbates the splash phenomenon of droplets, and the spray morphology assumes a "W" shape. With an increase in width and hypotenuse length, the spray shape appears as a "U" font. Among these, the influence of hypotenuse length on the spray shape exceeds that of the width.

3. Effects of width, height, and hypotenuse length on pressure distribution: A high-pressure region is formed

directly above the trapezoid, and the area of this region expands as the trapezoid width and hypotenuse length increase while decreasing as the height increases. Of these three dimensions, the change in hypotenuse length significantly influences the pressure distribution more than the width and height.

4. Effects of width, height, and hypotenuse length on characteristic parameters: The diameter of the crown is minimally affected by changes in width and hypotenuse length, but it increases with an increase in height. The crown's height diminishes as the width and hypotenuse length increase; as the hypotenuse length increases, the crown height decreases and then gradually increases. The cavity's base diameter expands with growing height and width expands with growing height and width, but the influence of width and height on the bottom diameter of the cavity decreases over time. In contrast, the hypotenuse length significantly affects the cavity's bottom diameter, which initially rises and subsequently falls as the hypotenuse lengthens.

ACKNOWLEDGEMENTS

This study is supported by the National Natural Science Foundation of China, the grant no is 62171206, we are deeply grateful for this funding.

CONFLICT OF INTEREST

Authors state the absence of any financial conflicts of

interest or personal connections that might be perceived to affect the research presented in this article.

AUTHORS CONTRIBUTION

Ying Li: Software usage, Writing the original manuscript, Methodology, Data curation; **Yangwei Lou:** Software usage, Visualization, Validation, Writing - review & editing and Data management; **Zifen He:** Software, Funding acquisition; **Menglian Liu:** Supervision.

REFERENCES

- Agrawal, S., Khurana, G., Samanta, D., & Dhar, P. (2023). Droplet post-impact regimes on concave contours. *The European Physical Journal. E, Soft Matter*, 46(10), 90. <https://doi.org/10.1140/epjc/s10189-023-00349-9>
- Alessandra, P. d. S., Fabiana, R. C., & Alexandre, R. M. F (2023). Spray-chilling system in the initial cooling process of swine half carcasses. *Meat Science*, 204, 109256. <https://doi.org/10.1016/j.meatsci.2023.109256>
- Bird, J., Dhiman, R., & Kwon, H. (2013). Reducing the contact time of a bouncing drop. *Nature*, 503(7476), 385-388. <https://doi.org/10.1038/nature12740>
- Chen, B. W., Wang, B., Mao, F., Tian, R. F., & Lu, C. (2020). Analysis of liquid droplet impacting on liquid film by CLSVOF. *Annals of Nuclear Energy*, 143. <https://doi.org/10.1016/j.anucene.2020.107468>
- Chen, D., Feng, A., Wu, F., Wang, T., & Lin, Z. (2024). Experimental study of the collision behavior between moving and sessile droplets on curved surfaces. *Chemical Engineering Science*, 299. <https://doi.org/10.1016/j.ces.2024.120530>
- Elhadi Ibrahim, M., & Medraj, M. (2019). Water droplet erosion of wind turbine blades: mechanics, testing, modeling and future perspectives. *Materials*, 13(1). <https://doi.org/10.3390/ma13010157>
- Fallah K, S., Passandidch-Fard, M., & Niazmand, H. (2016). Simulation of a single droplet impact onto a thin liquid film using the lattice Boltzmann method. *Journal of Molecular Liquids*, 222, 1172-1182. <https://doi.org/10.1016/j.molliq.2016.07.092>
- Guo, Y., Chen, G., Shen, S., & Zhang, J. (2015). *Double droplets simultaneous impact on liquid film*. IOP Conference Series: Materials Science and Engineering, 88. <https://doi.org/10.1088/1757-899x/88/1/012016>
- Guo, Y. L., Wang, F., Gong, L. Y., & Shen, S. Q. (2021). Numerical study of oblique droplet impact on a liquid film. *European Journal of Mechanics - B/Fluids*, 85, 386-396. <https://doi.org/10.1016/j.euromechflu.2020.07.006>
- Hirt, C. W. (1981). Volume of fluid (VOF) method for the dynamics of free boundaries. *Journal of Computational Physics*, 39(1), 201-225. [https://doi.org/https://doi.org/10.1016/0021-9991\(81\)90145-5](https://doi.org/https://doi.org/10.1016/0021-9991(81)90145-5)
- Hong, W., & Wang, Y. (2017). A coupled level set and volume-of-fluid simulation for heat transfer of the double droplet impact on a spherical liquid film. *Numerical Heat Transfer, Part B: Fundamentals*, 71(4), 359-371. <https://doi.org/10.1080/10407790.2017.1293960>
- Hu, Z., Chu, F., & Lin, Y. (2022). Contact Time of droplet impact on inclined ridged superhydrophobic surfaces. *Langmuir: The ACS Journal of Surfaces Colloids*, 38(4), 1540-1549. <https://doi.org/10.1021/acs.langmuir.1c03001>
- Hu, Z., Chu, F., & Shan, H. (2024). Understanding and utilizing droplet impact on superhydrophobic surfaces: phenomena, mechanisms, regulations, applications, and beyond. *Advanced Materials*, 36(11), e2310177. <https://doi.org/10.1002/adma.202310177>
- Kshitiz, K, S., & Song-Charng, K. (2022). Numerical study on the Leidenfrost behavior of a droplet stream impinging on a heated wall. *Physical Review. E*, 106(1-2), 015106. <https://doi.org/10.1103/PhysRevE.106.015106>
- Li, X. Y., Ma, X. D., & Lan, Z. (2010). Dynamic Behavior of the water droplet impact on a textured hydrophobic/superhydrophobic surface: The effect of the remaining liquid film arising on the pillars' tops on the contact time. *Langmuir*, 26(7), 4831-4838. <https://doi.org/10.1021/la903603z>
- Liang, G. T., Li, L., Chen, L. Z., Zhou, S. H., & Shen, S. Q. (2021). Impact of droplet on flowing liquid film: Experimental and numerical determinations. *International Communications in Heat and Mass Transfer*, 126. <https://doi.org/10.1016/j.icheatmasstransfer.2021.105459>
- Lin, S. L., Zhang, H., Wang, L. C., Lee, Y. Y., & Huang, C. E. (2023). Effects of fuel injection system and exhaust gas catalytic treatments on PAH emissions from motorcycles. *Environmental Science Pollution Research International*, 30(5), 13359-13371. <https://doi.org/10.1007/s11356-022-23042-4>
- Lin, Z., Zhang, H., Tao, J. Y., Jin, Y. Z., & Zhu, Z. H. (2022). Numerical Analysis of droplet impact on the convex surface with liquid film. *Langmuir*, 38(24), 7593-7602. <https://doi.org/10.1021/acs.langmuir.2c00742>
- Liu, X., Liu, L., Hu, Z., Li, R., & Wang, Z. (2024). Impact and freezing characteristics of deionized water droplets on cold curved surfaces. *International Journal of Fluid Engineering*, 1(4). <https://doi.org/10.1063/5.0226821>
- Liu, Y. H., Andrew, M., Li, J., Yeomans, J. M., & Wang, Z. K. (2015). Symmetry breaking in drop bouncing on curved surfaces. *Nature Communications*, 6(1). <https://doi.org/10.1038/ncomms10034>

- Lu, J., Qian, L., Liu, X., & Choi, Y. (2024). Characterization of energy loss in jet mechanism of a Pelton turbine. *International Journal of Fluid Engineering*, 1(3). <https://doi.org/10.1063/5.0209402>
- Manzello, S. L., & Yang, J. C. (2002). An experimental study of a water droplet impinging on a liquid surface. *Experiments in Fluids*, 32(5), 580-589. <https://doi.org/10.1007/s00348-001-0401-8>
- Ochowiak, M., Matuszak, M., & Włodarczak, S. (2017). The analysis of pneumatic atomization of Newtonian and non-Newtonian fluids for different medical nebulizers. *Drug Development Industrial Pharmacy*, 43(12), 1999-2010. <https://doi.org/10.1080/03639045.2017.1358274>
- Okawa, T., Shiraishi, T., & Mori, T. (2006). Production of secondary drops during the single water drop impact onto a plane water surface. *Experiments in Fluids*, 41(6), 965-974. <https://doi.org/10.1007/s00348-006-0214-x>
- Olsson, E., & Kreiss, G. (2005). A conservative level set method for two phase flow. *Journal of Computational Physics*, 210(1), 225-246. <https://doi.org/10.1016/j.jcp.2005.04.007>
- Olsson, E., Kreiss, G., & Zahedi, S. (2007). A conservative level set method for two phase flow II. *Journal of Computational Physics*, 225(1), 785-807. <https://doi.org/10.1016/j.jcp.2006.12.027>
- Osher, S. J. (1988). Fronts propagating with curvature-dependent speed: algorithms based on Hamilton-Jacobi formulations. *Journal of Computational Physics*, 79, 12-49. [https://doi.org/10.1016/0021-9991\(88\)90002-2](https://doi.org/10.1016/0021-9991(88)90002-2)
- Palmetshofer, P., Geppert, A. K., Steigerwald, J., Arcos, M. T., & Weigand, B. (2024). Thermocapillary central lamella recess during droplet impacts onto a heated wall. *Scientific Reports*, 14(1), 1102. <https://doi.org/10.1038/s41598-024-51382-3>
- Panzade, P., Wagh, A., Harale, P., & Bhilwade, S. (2024). Pharmaceutical cocrystals: a rising star in drug delivery applications. *Journal of Drug Targeting*, 32(2), 115-127. <https://doi.org/10.1080/1061186x.2023.2300690>
- Peng, X., Wang, T., Jia, F., Sun, K., Li, Z., & Che, Z. (2023). Singular jets during droplet impact on superhydrophobic surfaces. *Journal of Colloid Interface Science*, 651, 870-882. <https://doi.org/10.1016/j.jcis.2023.07.186>
- Rajendran, S., Jog, M. A., & Manglik, R. M. (2023). Predicting the Splash of a drop impacting a thin liquid film. *Langmuir : The ACS Journal of Surfaces*, 39(41), 14764-14773. <https://doi.org/10.1021/acs.langmuir.3c02185>
- Shi, J., Gong, L., Zhang, T., & Sun, S. (2022). Study of the Seawater desalination performance by electro dialysis. *Membranes*, 12(8). <https://doi.org/10.3390/membranes12080767>
- Sussman, M. (2000). A coupled level set and volume-of-fluid method for computing 3D and axisymmetric incompressible two-phase flows. *Journal of Computational Physics*, 162, 301-337. <https://doi.org/10.1006/jcph.2000.6537>
- Tao, J. Y., Chen, D. S., Lin, Z., & Zhu, Z. C. (2022). Numerical simulation analysis of symmetric impact of two droplets on a liquid film. *Physics of Fluids*, 34(9). <https://doi.org/10.1063/5.0110554>
- Theodorakakos, A., & Bergeles, G. (2004). Simulation of sharp gas-liquid interface using VOF method and adaptive grid local refinement around the interface. *International Journal for Numerical Methods in Fluids*, 45(4), 421-439. <https://doi.org/https://doi.org/10.1002/flid.706>
- Tsutsumi, A., C, Akutsu, S., K, Iwamiya, Y., & Terada, I., C. (2023). Antimicrobial surface processing of polymethyl methacrylate denture base resin using a novel silica-based coating technology. *Clinical oral Investigations*, 27(3), 1043-1053. <https://doi.org/10.1007/s00784-022-04670-z>
- Wal, R. V., Berger, G. M., & Mozes, S. D. (2005). The splash/non-splash boundary upon a dry surface and thin fluid film. *Experiments in Fluids*, 40(1), 53-59. <https://doi.org/10.1007/s00348-005-0045-1>
- Wang, A. B., & Chen, C. C. (2000). Splashing impact of a single drop onto very thin liquid films. *Physics of Fluids*, 12(9), 2155-2158. <https://doi.org/10.1063/1.1287511>
- Yada, S., Laci, U., Wijngaart, W., Lundell, F., Amberg, G., & Bagheri, S. (2022). Droplet impact on asymmetric hydrophobic microstructures. *Langmuir : The ACS Journal of Surfaces Colloids*, 38(26), 7956-7964. <https://doi.org/10.1021/acs.langmuir.2c00561>
- Yang, L., Xiang, J., Kang, H., Wang, X., Wen, C., & Rao, Z. (2024). Numerical investigations on compressible thermal flows in high-speed water entry. *International Journal of Fluid Engineering*, 1(3). <https://doi.org/10.1063/5.0219941>
- Yonemoto, Y., Tashiro, K., Shimizu, K., & Kunugi, T. (2022). Predicting the splash of a droplet impinging on solid substrates. *Scientific Reports*, 12(1), 5093. <https://doi.org/10.1038/s41598-022-08852-3>
- Zanin, A., Neves, D. C., & Teodoro, L. (2022). Reduction of pesticide application via real-time precision spraying. *Scientific Reports*, 12(1), 5638. <https://doi.org/10.1038/s41598-022-09607-w>